Reprinted from the preprint volume of SEVENTH CONFERENCE ON SATELLITE METEOROLOGY AND OCEANOGRAPHY June 6–10, 1994 Monterey, CA
Published by the American Meteorological Society, Boston, MA

P3.6

IDENTIFICATION AND CLASSIFICATION OF TRANSIENT SIGNATURES IN OVER-LAND SSM/I IMAGERY

Grant W. Petty*
Mark D. Conner

Purdue University
West Lafayette, Indiana

1 INTRODUCTION

Two distinct yet related factors make it difficult to reliably detect precipitation over land with passive microwave techniques, such as those developed during recent years for the Special Sensor Microwave/Imager (SSM/I).

The first factor is the general lack of contrast between radiances from the strongly emitting land background and that from a non-scattering atmosphere. Indeed, for certain common combinations of surface emissivity and temperature (both surface and atmospheric), significant changes in atmospheric opacity due to liquid water may have a negligible effect on satellite observed brightness temperatures, and whatever minor change occurs may be of either positive or negative sign. For this reason it is generally necessary for some degree of volume scattering by precipitation-size ice particles to be present in order to reduce the brightness temperature of the atmosphere relative to the warm background, by which process the precipitation may be observed.

Unfortunately, this requirement may not be met by all forms of precipitation; e.g., warm-cloud rain, which is not uncommon in the tropics or in regions of orographically induced rainfall. Furthermore, whatever modest scattering by ice is present in weaker cold-cloud (e.g., frontal stratiform) precipitation may be difficult to reliably distinguish as a consequence of the second complicating factor: namely, the usually strong spatial and temporal variability of emission from the land surface.

Traditionally, the approach used to address the latter problem in global over-land rainfall detection algorithms has entailed the development of empirical screening criteria, based on brightness temperature thresholds from various sensor channels, which can discriminate between precipitation and certain types of contaminating surface features such as wet soil, sand, cold bare ground, etc. Some algorithms (e.g., Adler et al. 1993; Grody 1991) have now apparently succeeded in greatly reducing the problem of false rain signatures from most types of surfaces by employing such screens.

Because large regional errors may enter into climatological rainfall estimates as a result of inadequately screened surface features, threshold-based screens must be geared toward the worst-case. If the thresholds are designed for global, or at least large-area use, this in turn implies that some sensitivity to lighter precipitation must be sacrificed. Furthermore, even with screening logic, snow cover presents a particular challenge because it closely mimics the frequency-dependent volume scattering features of frozen precipitation aloft.

The use of worst-case screening thresholds for global retrievals clearly handicaps the estimation of climatological rainfall over regions in which lighter stratiform precipitation predominates. This concern has motivated us to consider alternative approaches to the passive microwave observation of rainfall against a land background.

Here we describe exploratory new work in the detection of precipitation via transient changes in the microwave temperatures observed within a given geographic gridbox. The expectation is that this technique, by filtering out the quasi-permanent and slowly varying (in time) components of background emission, may significantly improve the detection of relatively light or weakly scattering precipitation events.

2 DIFFERENCING TECHNIQUE

The method under development begins with the remapping of all SSM/I channel brightness temperatures to an earth-referenced grid. Because

*Corresponding Author Address: Grant W. Petty, Earth and Atmospheric Sciences Dept., West Lafayette, IN, 47907-1397

SSM/I data swaths separated by 24 hours are only slightly displaced longitudinally from one another, the remapped grids from such a pair of swaths may be subtracted from one another to yield a reasonably wide swath of 24-hour brightness temperature *differences* in all seven channels, which we shall denote $\delta\vec{\mathbf{T}}$. To the extent that these differences are non-zero, they necessarily reflect short-term variations in surface emissivity, temperature, and/or meteorological conditions.

Some differences result from changes in snow cover or consistency, soil moisture, soil or vegetation temperature, while others are expected to be associated with precipitation. The spectral- and polarization-dependence of the 7-channel differences allows discrimination between some of these sources. For example, the appearance of standing water leads to an increase in the polarization of the surface emissivity, while increases in physical temperature are expected to lead to correlated increases in all 7 channels, though possibly with minor differences in magnitude for each channel. Volume scatterers, such as surface snow cover and precipitation aloft, are expected to lead to larger T_B depressions at high frequencies than at low frequencies and these depressions should be more or less independent of polarization.

To provide a basis for identifying and subtracting out the surface temperature component of the 24-hour difference signal, we computed separate monthly average brightness temperatures, at 0.25° latitude/longitude resolution, for morning and evening passes of the F-11 SSM/I for all twelve months of 1992. Obvious precipitation events were screened out based on the value of $T_{37V} - T_{85V}$. Systematic differences between the morning and evening averages at a given location can be attributed mainly to diurnal variations in temperature and, to a lesser extent, surface moisture.

The above morning-evening differences were pooled for all months and grid boxes over the United States and southern Canada and the 7×7 covariance matrix for all channels was computed. The first Principal Component (eigenvector) of this covariance matrix explained 89% of the total variance. The fact that all elements of this Principal Component are positive and of similar magnitude (Table 1) is consistent with its interpretation as a temperature response vector, which we shall denote $\hat{\mathbf{e}}_t$.

From the 24-hour swath differences, one may subtract out that portion of the variability corresponding to the empirically determined temperature response vector. That is, we derive a vector of temperature-corrected 7-channel differences at each location as follows:

$$\delta\vec{\mathbf{T}}' = \delta\vec{\mathbf{T}} - (\delta\vec{\mathbf{T}} \cdot \hat{\mathbf{e}}_t)\hat{\mathbf{e}}_t. \quad (1)$$

The filtered difference vectors $\delta\vec{\mathbf{T}}'$ are thus presumed to contain short-term brightness temperature variations not associated with surface temperature.

There remains the task of further filtering out that component of $\delta\vec{\mathbf{T}}'$ associated with other non-meteorological phenomena and thus isolating the component associated exclusively with precipitation (or phenomena spectrally indistinguishable from precipitation). For this purpose, Principal Component Analysis was again applied, this time to $\delta\vec{\mathbf{T}}'$ rather than to the monthly average morning-evening differences. The resulting first eigenvector again explains a sizable fraction of the total variance (76%); moreover it has a structure consistent with that expected for volume scatterers, in that the high and low frequency elements have opposite signs, while the difference between polarizations is minor. Designating this eigenvector as $\hat{\mathbf{e}}_p$, one may produce a final scalar "precipitation" field as

$$p = \hat{\mathbf{e}}_p \cdot \delta\vec{\mathbf{T}}'. \quad (2)$$

Table 1: Empirical temperature and precipitation response vectors

Channel	$\hat{\mathbf{e}}_t$	$\hat{\mathbf{e}}_p$
T_{19V}	0.365	0.271
T_{19H}	0.421	0.378
T_{22V}	0.338	0.199
T_{37V}	0.392	0.050
T_{37H}	0.441	0.137
T_{85V}	0.323	-0.542
T_{85H}	0.352	-0.655

3 EXAMPLE RESULTS

Figure 1 depicts the 85.5 GHz vertically polarized brightness temperature field observed on 4 November 1992 at approximately 12 UTC The most prominent feature is an area of depressed brightness temperature over much of the southeastern U.S. While this is clearly associated with precipitation, other regions of depressed brightness temperature, particularly over the Rocky Mountain states, are more difficult to classify and could be due to any of a number of surface variables. It is worth noting however that some of these features are as radiometrically cold as a good portion of the precipitation feature seen in the Southeast.

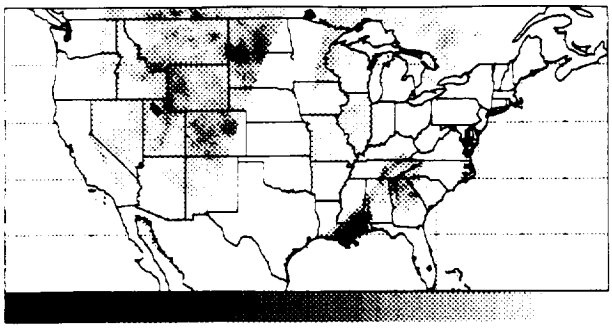

Fig. 1: Unfiltered 85.5 GHz vertically polarized T_B for 4 November 1992, approximately 12 UTC. Values range from 200 K (black) to 270 K (white).

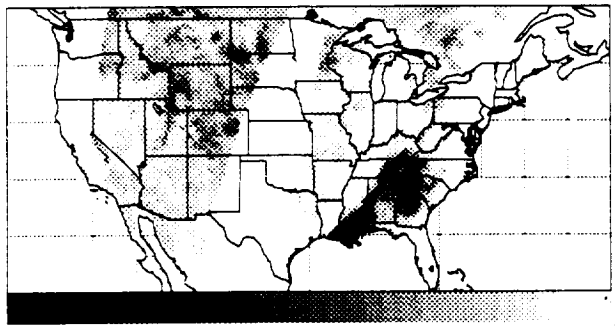

Fig. 2: $T_{37V} - T_{85V}$ for the same time as Fig. 1. Values range from 30 K (black) to −5 K (white).

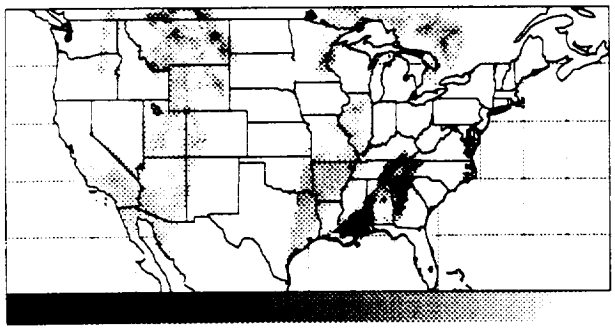

Fig. 3: 24-hour change in T_{85V} fields between 3 November and 4 November. Values range from −30 K (black) to 0 (white).

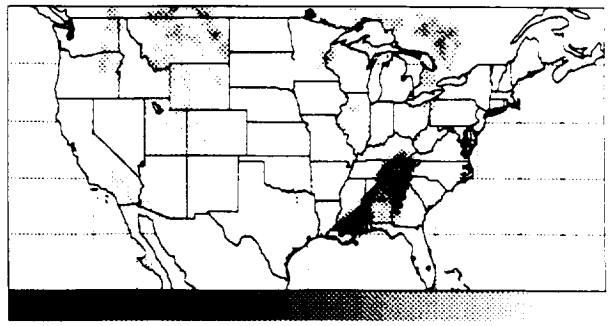

Fig. 4: Transient "precipitation" signal for 4 November, derived via Eq. (2). Units are arbitrary, but are scaled to give the same grayscale variance as in Fig. 3.

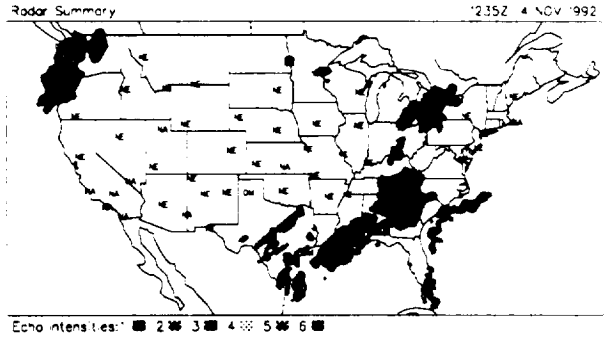

Fig. 5: Radar summary for 1235 UTC 4 November 1992, corresponding to the approximate time of the easternmost SSM/I swath in Figs. 1 and 2.

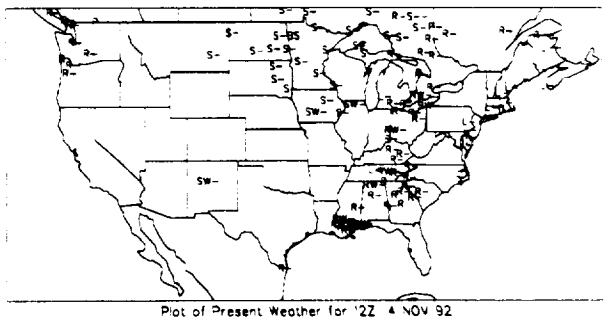

Fig. 6: Surface precipitation weather reports for 12 UTC 4 November 1992.

In order to discriminate volume scatterers — whose effect is strongly frequency-dependent — from other sources of depressed brightness temperatures, it is not uncommon to employ a frequency difference such as $T_{37V} - T_{85V}$. Figure 2 depicts the results of this approach. In general, the large precipitation feature is enhanced relative to the overall background signal; nevertheless, several features apparently associated with semi-permanent snow pack continue to stand out, particularly over the Sierra Nevada and Northern Rocky mountain ranges.

Figure 3 depicts the simple single-channel, 24-hour difference between the T_{85V} channels on 3 November and 4 November. This product highlights short-term temporal changes in brightness temperature while filtering out spatial variability associated mainly with surface type (only negative changes are shaded in this figure; positive changes appear as white). Features previously seen over the mountains of Utah, Wyoming, and California have now been largely suppressed, while others, including most conspicuously the precipitation feature, remain visible to varying degrees.

Figure 4 depicts the results of the application of (2) to the 7-channel, 24-hour differences. While the improvement is not spectacular, there is a significant strengthening of the precipitation feature relative to the background signal. Much of the remaining variability in the southern half of the U.S. is reduced to near zero.

All of these foregoing figures may be compared with Figs. 5 and 6, which depict the operational radar summary and surface hourly precipitation reports at the approximate time of the eastern SSM/I swath on 4 November. In general, it may be seen that the prominent feature in the SSM/I imagery is indeed associated with a region of widespread surface precipitaton. Several other areas of reported precipitation also appear to have counterparts in the filtered SSM/I imagery, for example over northeastern Ohio and southern Ontario, and over the border between Wisconsin and Minnesota.

Certain precipitation features, such as that reported over southwestern Ohio by both radar and surface observers, have no apparent signature in the SSM/I imagery. Conversely, other features appearing in the SSM/I but not in the conventional precipitation reports may perhaps be associated with changes in the properties of the surface snow cover.

In the summary, the use of 24-hour differences appears to remove much of the quasi-static background variability associated with different surface types. Further analysis of these multichannel differences, for example, using Principal Component Analysis, may facilitate the classification of transient features seen in microwave imagery and ultimately lead to improved discrimination of precipitation.

Acknowledgments

This work was supported in part by NASA Grant NAGW-2984. Capt. M.D. Conner's participation in this project is sponsored by the the Air Force Institute of Technology (AFIT).

REFERENCES

Adler, R.F., A.J. Negri, P.R. Keehn, and I.M. Hakkarinen, 1993: Estimation of monthly rainfall over Japan and surrounding waters from a combination of low-orbit microwave and geosynchronous IR data. *J. Appl. Meteor.*, **32**, 335–356

Grody, N.C., 1991: Classification of snow cover and precipitation using the Special Sensor Microwave Imager. *J. Geophys. Res.*, **96**, 7423–7435